



Dynamics of tungsten hexacarbonyl, dicobalt octacarbonyl, and their fragments adsorbed on silica surfaces

Kaliappan Muthukumar, Roser Valentí, and Harald O. Jeschke

Citation: *The Journal of Chemical Physics* **140**, 184706 (2014); doi: 10.1063/1.4873584

View online: <http://dx.doi.org/10.1063/1.4873584>

View Table of Contents: <http://scitation.aip.org/content/aip/journal/jcp/140/18?ver=pdfcov>

Published by the [AIP Publishing](#)

An advertisement for the journal 'Computing in Science & Engineering'. The background shows a row of computer monitors in a library or office setting, each displaying the journal's cover. The cover features a colorful, abstract image of a spiral or vortex. In the bottom right corner, the journal's logo 'computing in SCIENCE & ENGINEERING' is displayed in orange and white. Below the logo, the text 'AIP's JOURNAL OF COMPUTATIONAL TOOLS AND METHODS.' is written in a smaller, white, sans-serif font, followed by 'AVAILABLE AT MOST LIBRARIES.' in a large, bold, white, sans-serif font.

computing
in SCIENCE & ENGINEERING

AIP's JOURNAL OF COMPUTATIONAL TOOLS AND METHODS.
AVAILABLE AT MOST LIBRARIES.

Dynamics of tungsten hexacarbonyl, dicobalt octacarbonyl, and their fragments adsorbed on silica surfaces

Kaliappan Muthukumar, Roser Valentí, and Harald O. Jeschke
*Institut für Theoretische Physik, Goethe-Universität Frankfurt, Max-von-Laue-Straße 1,
60438 Frankfurt am Main, Germany*

(Received 11 February 2014; accepted 15 April 2014; published online 12 May 2014)

Tungsten and cobalt carbonyls adsorbed on a substrate are typical starting points for the electron beam induced deposition of tungsten or cobalt based metallic nanostructures. We employ first principles molecular dynamics simulations to investigate the dynamics and vibrational spectra of $W(CO)_6$ and $W(CO)_5$ as well as $Co_2(CO)_8$ and $Co(CO)_4$ precursor molecules on fully and partially hydroxylated silica surfaces. Such surfaces resemble the initial conditions of electron beam induced growth processes. We find that both $W(CO)_6$ and $Co_2(CO)_8$ are stable at room temperature and mobile on a silica surface saturated with hydroxyl groups (OH), moving up to half an Angström per picosecond. In contrast, chemisorbed $W(CO)_5$ or $Co(CO)_4$ ions at room temperature do not change their binding site. These results contribute to gaining fundamental insight into how the molecules behave in the simulated time window of 20 ps and our determined vibrational spectra of all species provide signatures for experimentally distinguishing the form in which precursors cover a substrate.
© 2014 AIP Publishing LLC. [<http://dx.doi.org/10.1063/1.4873584>]

I. INTRODUCTION

The study of the energetics and dynamics of individual molecules adsorbed on a substrate is relevant for several prominent fields of research such as molecular electronics,^{1,2} molecular magnetism,³ and catalysis.⁴ The possibility to manipulate individual molecules adsorbed on surfaces using the tip of a scanning tunneling microscope (STM) leads to an increasing need for theoretical information of the geometries as well as adsorption and desorption mechanisms and reaction pathways of adsorbates.⁵ STM probes can not only be used to arrange complex molecules on surfaces but also to measure their vibrational spectra.⁶ Molecules adsorbed on insulating surfaces which due to insufficient conductivity are hard to study by STM techniques have been investigated successfully using non-contact atomic force microscopy.⁷

Here, we will study molecules and substrates that are important in the context of electron beam induced deposition (EBID) of organometallic precursor molecules. This is a widely used method to grow size- and shape-controlled nanometer-sized structures.^{8–14} The obtained EBID deposits nevertheless possess a significant percentage of organic contaminants mainly from carbon and oxygen, lowering the conductivity of these deposits and thus limiting the possible applications of EBID.^{15–21} Several pre- and post-fabrication approaches have been employed to remove these contaminants, but reproducibility is still an issue. First principles calculations can provide a detailed description of the microscopic behavior of the deposits and are often used to improve the quality of the deposition processes. Important progress has been done, for instance, on atomic layer deposition^{22–26} and chemical vapor deposition^{27,28} processes.

Recently,^{29–31} in an attempt to understand the EBID growth process, we analyzed by means of density functional theory (DFT) calculations the interaction of precursors like $W(CO)_6$, $Co_2(CO)_8$, and $CH_3(C_5H_5)Pt[CH_3]_3$ on two different SiO_2 surfaces (fully and partially hydroxylated) as a representative for untreated and pretreated EBID surfaces (hereafter, surfaces corresponds to SiO_2 surfaces unless otherwise mentioned). These studies illustrate the preferred orientation of the adsorbate and the nature of the interaction between the precursor molecules and the SiO_2 substrates. Further, interesting phenomena such as the spontaneous fragmentation of the carbonyl precursors ($W(CO)_6$ to $W(CO)_5$ and $Co_2(CO)_8$ to two $Co(CO)_4$ molecules) on the partially hydroxylated surfaces that correspond to pre-treated surfaces were observed.^{30,31}

It has recently been reported that the surface residence time of an organometallic precursor should be sufficiently long (lasting from microseconds to milliseconds) to have an efficient deposition yield.¹⁷ In order to understand these observations and to improve the conditions for the adhesion of precursor molecules to the substrate, it is essential to have knowledge on the behavior of the precursor molecules and their fragments on the surface SiO_2 substrates. Theoretical and experimental studies focussing on the adsorption process of free CO on various surfaces and several molecules on different SiO_2 substrates have been reported.^{32–35} However, little is known on the dynamics of $W(CO)_6$ and $Co_2(CO)_8$ precursors and their fragments on SiO_2 surfaces. Therefore, in this work we use first principles molecular dynamics simulations to investigate the nature of $W(CO)_6$ and $Co_2(CO)_8$ molecule adsorption on fully and partially hydroxylated SiO_2 surfaces and provide quantitative microscopic insight into the stability of these fragmented precursors on these surfaces and on their vibrational spectra.

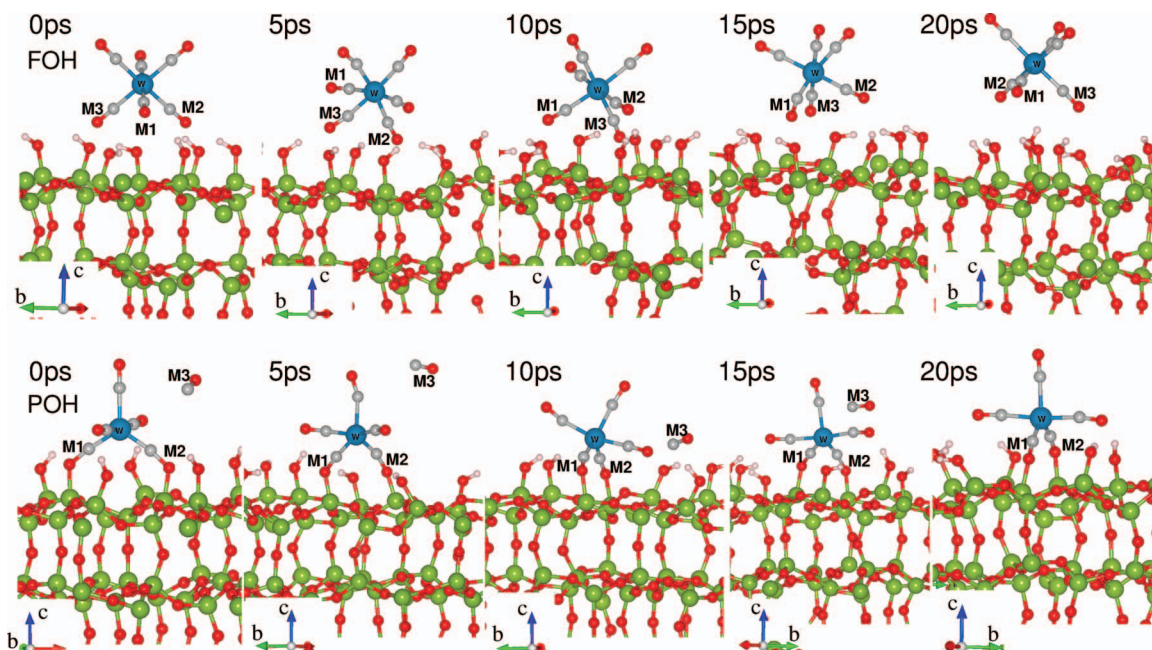


FIG. 1. Adsorption of $W(CO)_6$ on fully hydroxylated (FOH, upper panel) and partially hydroxylated (POH, lower panel) substrates. The illustrated snapshots are the configurations taken at every 5 ps interval. Color code: Green - Si, Red - O, light Blue - W, Gray - C, and Magenta - H throughout this manuscript. M1, M2, and M3 are the labels for specific ligands to identify the changes in 2D view and the snapshots have slightly different orientations (note the coordinate axis) to better display the changes happening to the system.

II. COMPUTATIONAL DETAILS

Ab initio molecular dynamics (MD) simulations were performed in the framework of DFT. We employed the projector augmented wave (PAW) basis^{36,37} within the generalized gradient approximation in the parametrization of Perdew, Burke, and Ernzerhof (PBE) as implemented in VASP.^{37–40} Spin polarized calculations including the corrections for long range van der Waals interactions^{37,38} were used in all calculations. All ions were relaxed using the conjugate gradient scheme until the forces were reduced by $\lesssim 0.01$ eV/Å with a plane wave energy cut-off of 400 eV. The Brillouin zone for the substrate-precursor complex was sampled at the gamma point only.

The structures considered as initial configurations for the MD simulations are shown in Figs. 1 and 5 (see the $t = 0$ ps snapshot). MD simulations were performed for 20 ps on a canonical ensemble at a finite temperature of $T = 298$ K using the Nose-Hoover thermostat.⁴¹ The temperature was chosen in accordance with the reported experimental results where the largest temperature rise during $W(CO)_6$ deposition was 1°C when a 1.42 nA electron beam was used for depositing tungsten nanostructures.^{42,43} The Verlet algorithm in its velocity form with a time step of $\Delta t = 1$ fs was used to integrate the equations of motion. We also performed MD simulations for the precursor molecules ($W(CO)_6$ and $Co_2(CO)_8$) in the gas phase by placing the molecules in a cubic box of $a = b = c = 30$ Å using similar parameters as for the substrate-precursor complex. The length of the simulation for the molecule was limited to 10 ps.

The power spectrum $I(\omega)$ provides information about the distribution of the vibrational energy of the system. It can be computed by a Fourier transformation of the velocity autocorrelation function obtained from the velocities $\mathbf{v}_i(t)$ of all

atoms in the course of the MD trajectory. The method we use is described in the Appendix. Initially, we have compared the vibrations of the gas phase precursor molecules obtained by the finite displacement method with the calculated power spectrum (vibrations through the finite displacement method were computed for the precursor molecules $W(CO)_6$ and $Co_2(CO)_8$ in the gas phase using Turbomole 6.0.^{44–46} The geometries were optimized using triple ζ basis sets for all elements and we used an effective core potential (60 core electrons) for W in the case of $W(CO)_6$.⁴⁷ The vibrations computed by these two methods agree with each other and are explained in Sec. III C. Therefore, vibrations for the SiO_2 substrate and the complex precursor molecule-substrate have been evaluated only from the power spectrum so as to reduce the computational effort in computing the Hessian matrix.

III. RESULTS

A. Dynamics of $W(CO)_6$ on SiO_2 surfaces

Previous DFT calculations³⁰ indicate that $W(CO)_6$ interacts through weak physisorption with surface hydroxyls on the fully hydroxylated surface and by strong chemisorption on the Si sites available on partially hydroxylated surfaces with substantial changes in the structure and electronic properties. The most stable configuration of $W(CO)_6$ on fully hydroxylated has an adsorption energy of -0.498 eV while the fragment $W(CO)_5$ together with a free CO ligand stabilize with an energy -1.262 eV on a partially hydroxylated surface. In Fig. 1 we show five snapshots in 5 ps intervals of the MD simulations of $W(CO)_6$ on a fully hydroxylated surface (upper panel) and of the fragment $W(CO)_5$ together with a free CO ligand on a partially hydroxylated surface (lower panel).

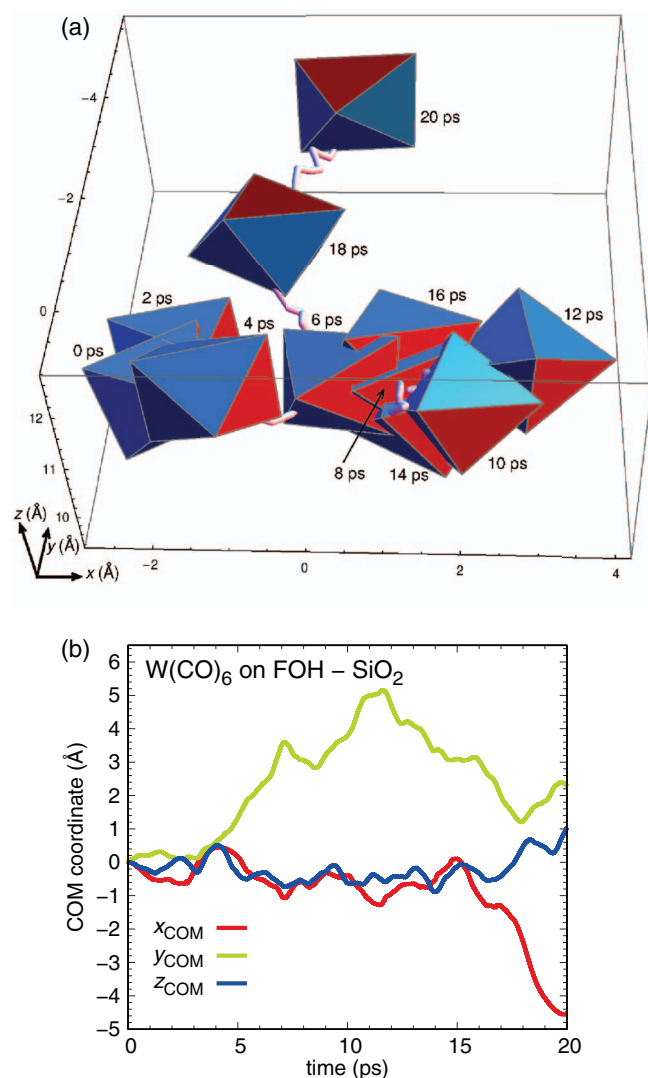


FIG. 2. Schematic illustration of the movement of $W(CO)_6$ on a fully hydroxylated surface. In the top panel, the polygon of the oxygen atoms of $W(CO)_6$ is shown, with one facet always shown in red in order to visualize the rotations of the molecule. In the lower panel the time evolution of the three center-of-mass (COM) coordinates of $W(CO)_6$ is shown. FOH in the figure corresponds to the fully hydroxylated surface.

Analysis of the trajectory in the fully hydroxylated case indicates that the $W(CO)_6$ molecule exhibits a considerable drift and moves around the initial binding sites in a fully hydroxylated surface. In order to visualize this drifting, Fig. 2 shows a schematic depiction of the $W(CO)_6$ displacement together with the center-of-mass (COM) analysis. The calculated drifting distance on the surface after 20 ps is ~ 5 Å. These simulations illustrate that the undissociated $W(CO)_6$ molecule changes the orientation considerably but does not desorb away from the fully hydroxylated surface.

However, a chemisorbed $W(CO)_5$ molecule which is formed by the release of a CO ligand from $W(CO)_6$ (Fig. 1, lower panel) remains localized on its binding site on a partially hydroxylated surface. The dissociated CO ligand does not recombine with the parent moiety and the vacant site on W remains empty and is not filled by surface hydroxyls as has been suggested as a possibility for $Mo(CO)_5$.⁴⁹ It should be noted that $W(CO)_5$ in the gas phase is stable on a square

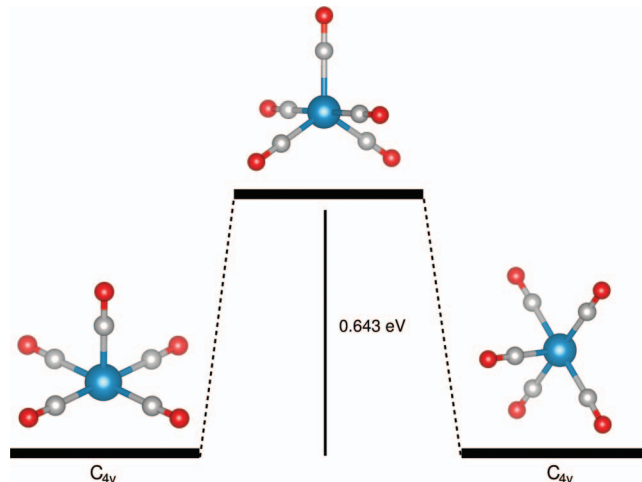


FIG. 3. DFT optimized structure of $W(CO)_5$. In the gas phase it possess a C_{4v} symmetric structure. The trigonal bipyramidal structure (middle panel) is 0.643 eV less stable than the square pyramidal structure (left and right panels)⁴⁸ but it is stabilized by surface-molecule interaction on partially hydroxylated surface.

pyramidal structure and different conformations are possible through the pathway shown in Fig. 3 involving a trigonal bipyramidal transition state.⁵⁰ Analysis of the adsorbed $W(CO)_5$ structure (compare the transition state on Fig. 3 with the configuration at 0 ps in Fig. 1, lower panel) indicates that the $W(CO)_5$ molecule is stabilized in a trigonal bipyramidal structure on partially hydroxylated surfaces. The stabilization of such a transient intermediate has been proposed for $Cr(CO)_5$ and the present work supports such a proposal also for $W(CO)_5$.⁵¹ This stabilization should have an impact over the kinetics of further release of intra molecular CO ligands.

Evaluation of the changes in the WC and CO bond lengths of the adsorbates $W(CO)_6$ and $W(CO)_5$ (see Fig. 4) during the first 20 ps of the trajectory shows deviations from the initial configuration of the order of 1%-2% and are due to thermal fluctuations. We will analyze these deviations in more detail in Sec. III C. The electronic structure of the final configurations of the complex molecule-substrate on both fully and partially hydroxylated cases shows only minor variations with respect to the initial configurations (results not shown).

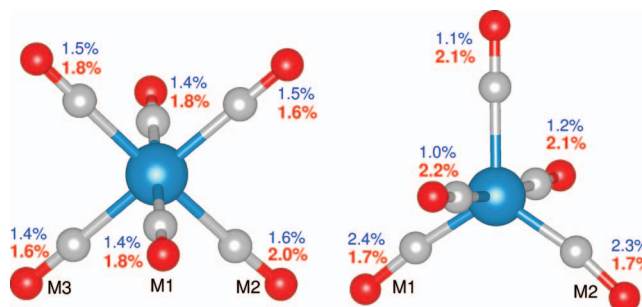


FIG. 4. Variations in the structural features of $W(CO)_6$ on SiO_2 surfaces on fully hydroxylated (left panel) and partially hydroxylated (right panel). Bold (red) letters correspond the WC and normal letters (blue) to the CO bond. The values shown in this figure are the standard deviation of the respective values in the initial structure.

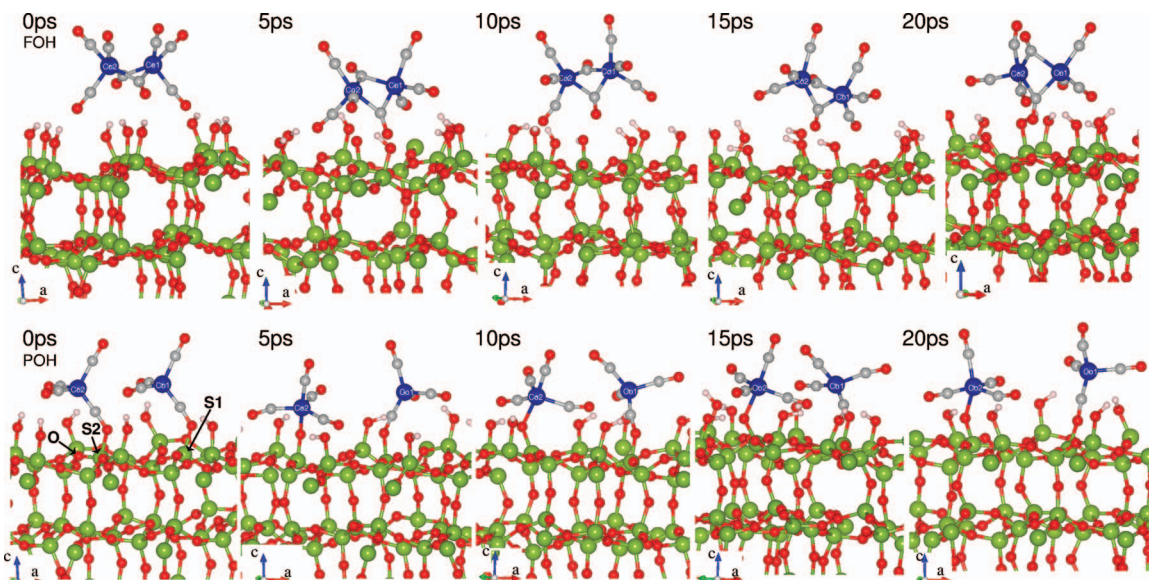


FIG. 5. Adsorption of $\text{Co}_2(\text{CO})_8$ on fully hydroxylated (top) and partially hydroxylated (POH) substrates. The illustrated snapshots are the configurations taken at every 5 ps interval. S1 and S2 in partially hydroxylated case denotes the two bonding sites on the surface where $\text{Co}(\text{CO})_4$ fragments are bonded. Color code: Blue - Co, throughout this manuscript. The orientation of the configuration is denoted by the coordinate system on the bottom left-hand side of each panel.

B. Dynamics of $\text{Co}_2(\text{CO})_8$ on SiO_2 surfaces

We now proceed with the adsorption scenario of $\text{Co}_2(\text{CO})_8$ interacting with SiO_2 surfaces. In Ref. 31 a weak bonding of $\text{Co}_2(\text{CO})_8$ on fully hydroxylated surfaces was observed, similar to the case of $\text{W}(\text{CO})_6$, with an adsorption energy of -0.76 eV. In contrast, $\text{Co}_2(\text{CO})_8$ molecules on a partially hydroxylated surface fragment into two $\text{Co}(\text{CO})_4$ moieties rather than eliminating a CO ligand as in the case of $\text{W}(\text{CO})_6$. The fragmented $\text{Co}(\text{CO})_4$ moieties exhibit a strong chemisorption on partially hydroxylated surfaces with an adsorption energy of -1.77 eV.³¹ Considering the above configurations as the initial setting for our MD simulations, Fig. 5 shows snapshots in 5 ps intervals of $\text{Co}_2(\text{CO})_8$ adsorbed on a fully hydroxylated surface (upper panel) and of $\text{Co}(\text{CO})_4$ fragments adsorbed on a partially hydroxylated surface (lower panel).

We observe a significant drift of $\text{Co}_2(\text{CO})_8$ on the fully hydroxylated surface but as this is a larger molecule than $\text{W}(\text{CO})_6$, the displacement is less pronounced than in $\text{W}(\text{CO})_6$. This can be seen by comparing Fig. 6, where the COM movement of $\text{Co}_2(\text{CO})_8$ on a fully hydroxylated surface is depicted, with Fig. 2(b) which is analogous to $\text{W}(\text{CO})_6$. The calculated drifting radius of $\text{Co}_2(\text{CO})_8$ within 20 ps is about 4 Å.

We now investigate the adsorption of the $\text{Co}(\text{CO})_4$ species on partially hydroxylated surfaces (Fig. 5, lower panel). We would like to note that, unlike in the case of $\text{W}(\text{CO})_5$, the $\text{Co}(\text{CO})_4$ species in the gas phase possesses a tetrahedral structure which remains stable with a slight distortion on the partially hydroxylated surfaces (see $t = 0$ ps in Fig. 5, lower panel). During the MD simulations, the fragmented $\text{Co}(\text{CO})_4$ species are localized on the surface but we observe severe changes in the orientation of CO ligands. In particular, we find that the $\text{Co}(\text{CO})_4$ fragment bonded to the S2 site on the partially hydroxylated surface as shown in Fig. 5 (lower panel) shows bonding of the Co atom to sur-

face oxygen as time evolves (compare $t = 0$ ps and $t = 5$ ps snapshots). A similar situation was suggested by Rao *et al.*⁵² during the adsorption of $\text{Co}_2(\text{CO})_8$ on dehydroxylated MgO and on SiO_2 surfaces. However, within our simulation window, we only observe this effect for the $\text{Co}(\text{CO})_4$ fragment bonded to the S2 site but not for the fragment bonded to the S1 site (see Fig. 5, lower panel) of the partially hydroxylated SiO_2 surfaces. Such a metal-substrate bond might be due to activation of the substrate surface by dehydroxylation.

C. Vibrations of $\text{W}(\text{CO})_6$ and $\text{Co}_2(\text{CO})_8$ on a SiO_2 surface

1. $\text{W}(\text{CO})_6$ adsorbed on SiO_2 surface

We first start with the analysis of the vibrational spectrum of $\text{W}(\text{CO})_6$ in the gas phase and the modes arising due to SiO_2 surfaces. We observe $\text{W}-\text{C}$ stretching modes

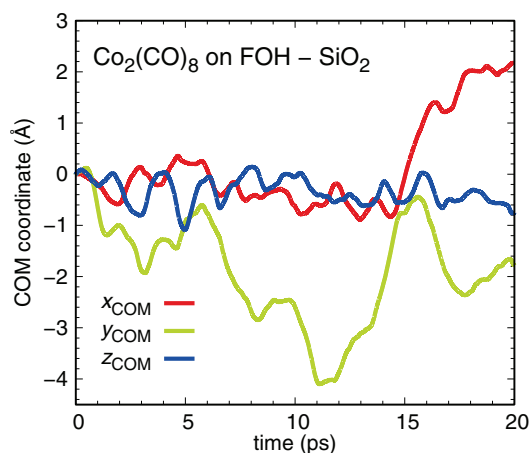


FIG. 6. Evolution of the three center-of-mass coordinates of $\text{Co}_2(\text{CO})_8$ adsorbed on a fully hydroxylated surface during the 20 ps trajectory.

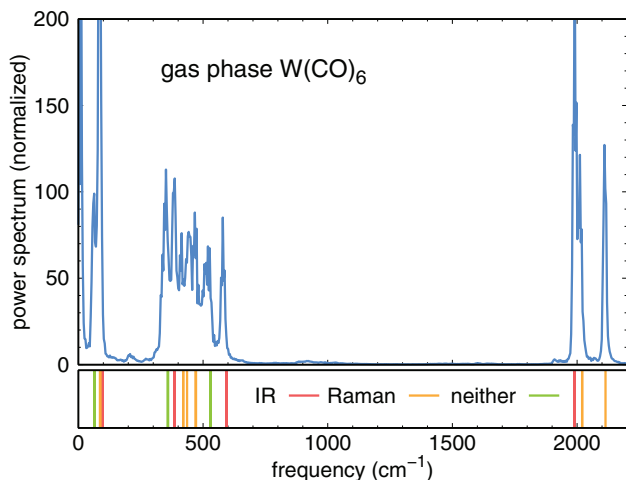


FIG. 7. Calculated vibrational spectrum of the gas phase of $W(CO)_6$ molecules by Fourier transforming the velocity autocorrelation function obtained from the MD trajectory (upper panel) and by the finite displacement method (lower panel).

and $(OC)-W-(CO)$ bending modes at $300-600\text{ cm}^{-1}$, and $C-O$ stretching modes at $1900-2150\text{ cm}^{-1}$ for the gas phase $W(CO)_6$. The bending vibrations that involve $W-(CO)$ atoms are seen at $60-100\text{ cm}^{-1}$. All these normal modes are seen in both upper (power spectrum) and lower panel (finite displacement method) of Fig. 7. Also, in Fig. 8, we compare the power spectrum calculated for $W(CO)_6$ adsorbed on a fully hydroxylated surface with experimental infrared and Raman spectra measured for SiO_2 substrates so as to analyze the vibrations of SiO_2 .^{53,54} We observe a good overall agreement between the calculated SiO_2 modes (infrared and Raman active peaks at $100-200$, $400-450$, $700-800$, and $1000-1100\text{ cm}^{-1}$) and the experimental spectrum.^{55,56} Apart from SiO_2 modes, the additional modes in Fig. 8 are due to the surface adsorbed $W(CO)_6$ molecule (compare with Fig. 7). This

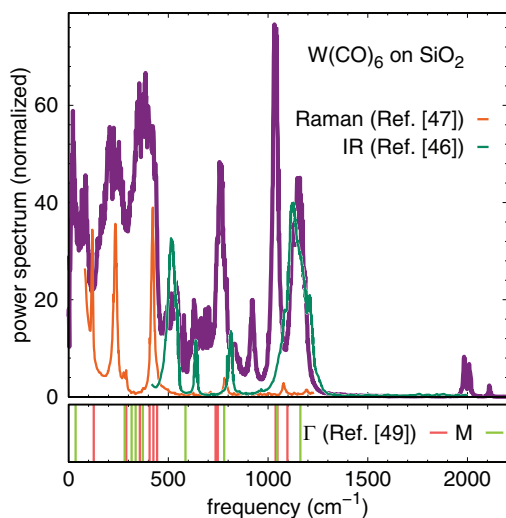


FIG. 8. Comparison of the calculated power spectrum for $W(CO)_6$ adsorbed on fully hydroxylated with the experimentally measured infrared and Raman spectrum^{53,54} for the SiO_2 substrate. In the lower panel, the vibrational frequencies of β cristobalite at Γ and M points in the Brillouin zone as calculated in Ref. 56 are shown.

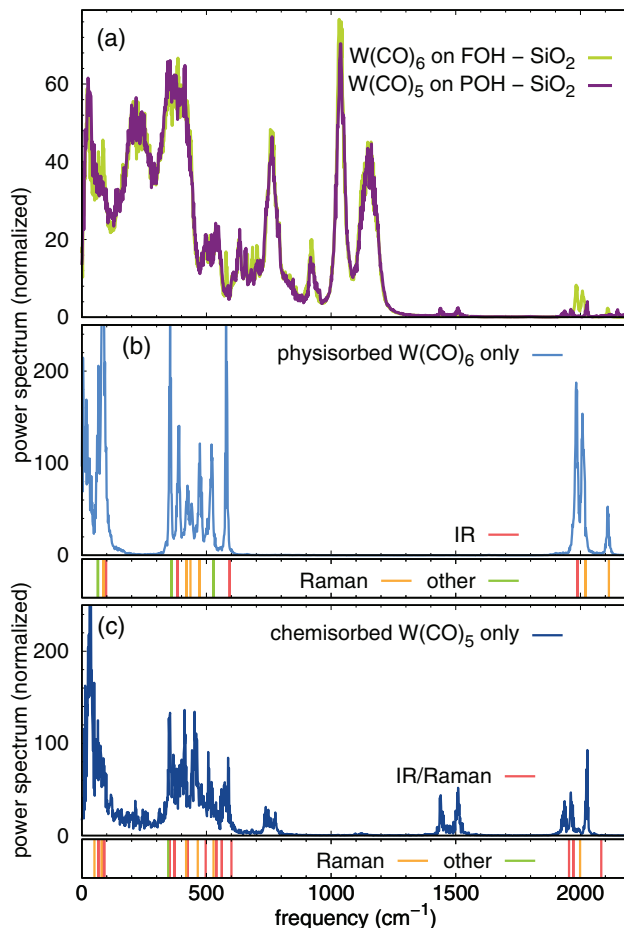


FIG. 9. (a) Comparison of the total power spectrum for (i) $W(CO)_6$ on a fully hydroxylated surface and (ii) $W(CO)_5$ on a partially hydroxylated surface. (b) Power spectrum of the physisorbed $W(CO)_6$ only in case (i) compared to the vibrational modes of $W(CO)_6$ in the gas phase. The modes are classified in Raman, infrared, and other. (c) Power spectrum of the chemisorbed molecule $W(CO)_5$ only in case (ii) compared to the vibrational modes of $W(CO)_5$ in the gas phase.

analysis indicates that the adopted methodology to calculate the power spectrum could be used to describe the vibrations of $W(CO)_6$ adsorbed on SiO_2 surfaces.

In Fig. 9 we present the total power spectrum of $W(CO)_6$ adsorbed on fully and partially hydroxylated surfaces (Fig. 9(a)) and only the vibrations of physisorbed $W(CO)_6$ and chemisorbed $W(CO)_5$ extracted from it which are compared with the vibrations (obtained by finite displacement method, shown as vertical bars) of isolated gas phase structures (Figs. 9(b) and 9(c)). From Fig. 9(b), we observe only minor changes in the vibrational modes of $W(CO)_6$. In particular, the CO frequencies observed between 1900 and 2110 cm^{-1} (two of which are Raman active) for the gas phase of $W(CO)_6$ have also been observed upon its bonding to fully hydroxylated surfaces without being perturbed indicating that the molecule retains its gas-phase characteristics. These features are indeed similar to $W(CO)_6$ adsorbed on hydroxylated alumina ($\gamma-Al_2O_3$) surfaces where all the molecular vibrations are retained^{57,58} indicating the weak interaction between $W(CO)_6$ and the substrate.

From the analysis of the chemisorbed $W(CO)_6$ fragments on partially hydroxylated surfaces (see Fig. 9(c)) we find, in

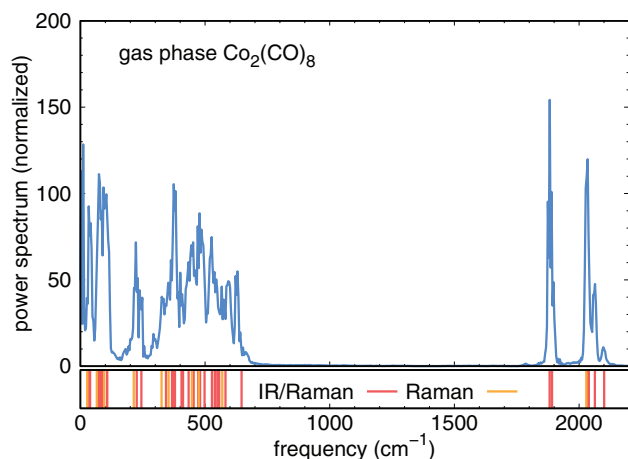


FIG. 10. Calculated vibrational spectrum of the gas phase of $\text{Co}_2(\text{CO})_8$ molecules by Fourier transforming the velocities obtained from the MD trajectory (upper panel) and by the finite displacement method (lower panel).

addition to the shifts of several peaks, two new modes occurring at $700\text{--}800\text{ cm}^{-1}$ and $1400\text{--}1600\text{ cm}^{-1}$. Peaks at $700\text{--}800\text{ cm}^{-1}$ which correspond to the Raman vibrations of β -cristobalite,⁵⁵ are now seen, because of precursor bonding to the surface. Also, the peaks at $1400\text{--}1600\text{ cm}^{-1}$ appear as a result of oxygen (of CO) interaction with substrate Si atoms.^{58,59} Due to this interaction the bonding between tungsten and the carbonyl in $\text{W}(\text{CO})_6$ gets affected leading to a considerable split of peaks in the regions that correspond to the vibrations of C–O ($1900\text{--}2100\text{ cm}^{-1}$) and W–C ($300\text{--}600\text{ cm}^{-1}$) bonds of $\text{W}(\text{CO})_6$, respectively.

2. $\text{Co}_2(\text{CO})_8$ adsorbed on SiO_2 surface

There have been some studies aimed at understanding the vibrations of $\text{Co}_2(\text{CO})_8$ adsorbed on SiO_2 . However they are either limited to the carbonyl region of the spectrum^{52,60} or they observe immediate conversion of $\text{Co}_2(\text{CO})_8$ to subcarbonyl species.^{61,62} We first show in Fig. 10 the analysis of the vibrational spectrum of $\text{Co}_2(\text{CO})_8$ in the gas phase from power spectrum and the finite displacement method and both methods agree with each other and the existing reports.⁶³ The two sets of vibrations in the region $1850\text{--}1900$ and $2100\text{--}2000\text{ cm}^{-1}$ are assigned to the stretching modes of the bridging and terminal CO ligands and the Co–Co stretching mode in $\text{Co}_2(\text{CO})_8$ is observed between $200\text{--}250\text{ cm}^{-1}$.

We now investigate the vibrations of $\text{Co}_2(\text{CO})_8$ adsorbed on SiO_2 by analyzing the power spectrum. In Fig. 11(a) we show the power spectrum of $\text{Co}_2(\text{CO})_8$ on a fully hydroxylated surface compared to the power spectrum of $\text{Co}(\text{CO})_4$ fragments on a partially hydroxylated surface. The extracted vibrations of physisorbed $\text{Co}_2(\text{CO})_8$ and chemisorbed $\text{Co}(\text{CO})_4$ from the total power spectrum are compared with the vibrations of the isolated molecules and are shown in Figs. 11(b) and 11(c), respectively. The results illustrate that $\text{Co}_2(\text{CO})_8$ on fully hydroxylated surface preserves the gas-phase molecule characteristics (cf. Figs. 10 and 11(b)).

In the case of $\text{Co}(\text{CO})_4$ on partially hydroxylated surfaces, the overall agreement of the power spectrum with that

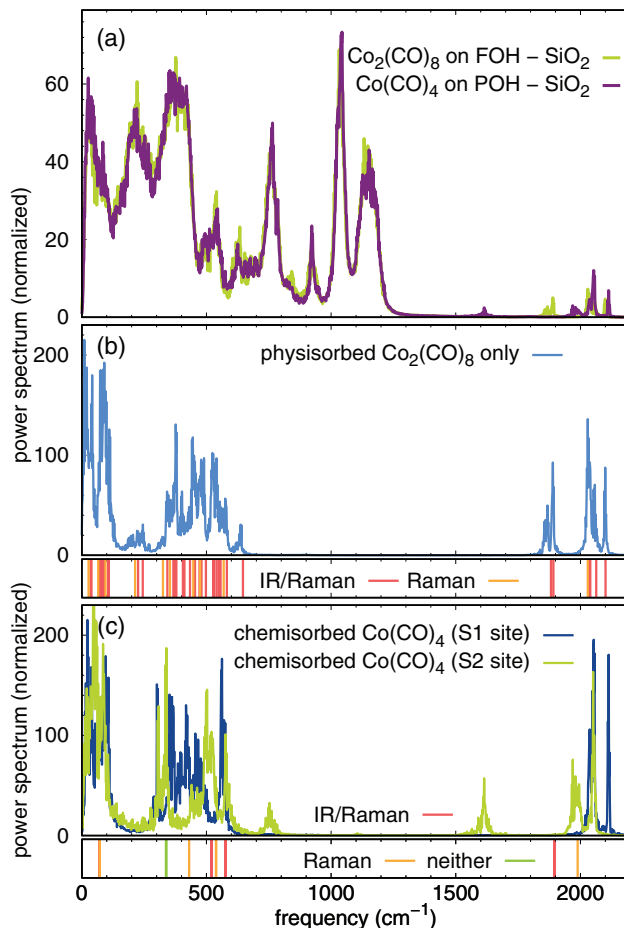


FIG. 11. (a) Comparison of the total power spectrum for (i) $\text{Co}_2(\text{CO})_8$ on a fully hydroxylated surface and (ii) the two $\text{Co}(\text{CO})_4$ fragments on a partially hydroxylated surface. (b) Power spectrum of the physisorbed molecule $\text{Co}_2(\text{CO})_8$ in case (i) compared to the vibrational modes of $\text{Co}_2(\text{CO})_8$ in the gas phase. (c) Power spectrum of the chemisorbed $\text{Co}(\text{CO})_4$ fragments in case (ii) compared to the vibrational modes of $\text{Co}(\text{CO})_4$ in the gas phase.

of the gas phase $\text{Co}(\text{CO})_4$ moiety is relatively poor because the $\text{Co}(\text{CO})_4$ moieties exhibit strong structural distortions upon bonding to the SiO_2 substrate which is absent in the gas phase computations. In the power spectrum, we find that the modes in the region $220\text{--}250\text{ cm}^{-1}$ (Co–Co stretching) and the mode at approximately 1850 cm^{-1} (bridging carbonyls) disappear owing to the fact that the $\text{Co}_2(\text{CO})_8$ molecule fragments on partially hydroxylated surfaces. Further, two new modes in the $600\text{--}800\text{ cm}^{-1}$ and $1400\text{--}1600\text{ cm}^{-1}$ regions appear in this case (cf. Figs. 11(a) and 11(c)) illustrating the interaction of surface Si atoms with the carbonyls through the oxygen atom of the CO. However, this situation is only observed for one of the $\text{Co}(\text{CO})_4$ moieties indicating that the fragmented species behave differently. This is a consequence of the interaction of surface oxygen atoms with the Co atom observed for the fragment bonded to the S2 site (see Fig. 5).

D. Discussion

Investigation of surface adsorption and residence-time of the precursors on the surface is necessary for improving the understanding of deposition processes. The present study

elucidates the vibrational footprints of precursors which interact through weak physisorption with fully hydroxylated surfaces and by strong chemisorption with partially hydroxylated surfaces.

The authors of Ref. 64 found that physisorbed $W(CO)_6$ molecules on TiO_2 surfaces completely desorb when the system is cooled down to room temperature. Our study finds no desorption of $W(CO)_6$ molecules on fully hydroxylated surfaces in the considered length of simulation. Also, $Co_2(CO)_8$ molecules on fully hydroxylated surfaces were reported to fragment spontaneously^{61,65} but, in our calculations on fully hydroxylated surfaces we did not observe any tendency to fragmentation or an indication of chemisorption. Other effects (probably extrinsic) may be responsible for the experimental observations.

The bond variations of $W(CO)_6$ and $Co_2(CO)_8$ adsorbed on fully hydroxylated surfaces indicate uniform fluctuations ($W-C$ and $C-O$ bonds) on either side (i.e., oriented towards the surface and the vacuum) of the molecule. On the contrary, the relative bond values of $W(CO)_5$ on partially hydroxylated surfaces show non-uniform variations indicating that certain bonds (i.e., $W-C$ bonds oriented towards the vacuum and the CO bonds towards the substrate) experience larger changes than others. Thus, for favorable conditions, the bond between C and O for the CO bonded to the surface might cleave leaving the surface Si atoms terminated with oxygens. This situation is not observed in the present MD simulations but the higher ratio of carbon contamination with respect to oxygen (before atmospheric air exposure) in the EBID-obtained samples¹⁷⁻²¹ is an indication that some processes involving CO bond breaking must play a role. Similarly, we found in the case of $Co_2(CO)_8$ on partially hydroxylated surfaces, that surface oxygen atoms are involved in bonding to the dissociated surface species. This suggests that the removal of oxygen components from the deposits might not be an easy task to achieve. Presence of oxygen contamination is also expected to occur as a result of exposure of EBID deposits to the air. Thus the composition of the EBID deposits is determined to a large extent by the number of available active Si sites (alternatively the degree of hydroxylation), the frequency of these precursor molecules approaching such a site, and the exposure time to the environments. Furthermore, the surface defects observed in SiO_2 during the interaction of $Co(CO)_4$ with partially hydroxylated surfaces might also act as an active site for activating the approaching precursor molecule that could account for the facile dissociation of $Co_2(CO)_8$ on SiO_2 .^{31,66}

On partially hydroxylated surfaces our results for both $W(CO)_6$ and $Co_2(CO)_8$ show that the fragmented species remain localized, thus blocking active sites on the surface.

IV. CONCLUSIONS

The purpose of this work was to model by means of *ab initio* molecular dynamics simulations the dynamics of two precursor molecules adsorbed on fully and partially hydroxylated SiO_2 surfaces in order to achieve a better understanding of the microscopics of electron-beam induced deposition of nanostructures. Our results reveal that $W(CO)_6$ and $Co_2(CO)_8$ molecules preserve their gas-phase bonding characteristics on

fully hydroxylated surfaces. Apart from a considerable drift, only minor variations in the structure and vibrations is observed. Therefore spontaneous dissociation of these precursor molecules will not be possible on fully hydroxylated surfaces, unless some surface active sites are created by external forces.

For the case of $W(CO)_6$ and $Co_2(CO)_8$ on partially hydroxylated surfaces, the fragmented species retain the chemisorbed character on the surface and we do not observe any reformation of the parent precursor moiety, but instead a slight tendency towards fragmentation. We also observe a smaller weakening of the surface-oriented CO bonds compared to vacuum-oriented CO bonds in $W(CO)_6$ and $Co_2(CO)_8$ on partially hydroxylated surfaces. Therefore, conditions that favor the formation of active sites (in this case surface Si atoms) are needed in order to have high efficiency in fragmentation and improve the metal content of the deposit.

The calculated vibrational spectra of these carbonyl molecule/ SiO_2 substrate systems show clear fingerprints to be detected experimentally. We propose therefore the consideration of such simulations as a route to experimentally distinguish the form in which precursors cover a substrate.

Finally, while the present simulations provide insights on the surface-precursor interaction, the investigation of other processes like surface-electron, precursor-electron, and deposit-molecule interaction remains a challenge for future work.

ACKNOWLEDGMENTS

We would like to thank the Beilstein-Institut, Frankfurt/Main, Germany, within the research collaboration NanoBiC for financial support. The generous allotment of computer time by CSC-Frankfurt and LOEWE-CSC is also gratefully acknowledged.

APPENDIX: ESTIMATION OF THE POWER SPECTRUM

We use the power spectrum for analysing the vibrational characteristics of precursor molecules in the gas phase and for the entire system of precursors chemi- or physisorbed on a silica substrate.⁶⁷ The power spectrum is defined as^{68,69}

$$I(\omega) = \frac{1}{2\pi} \int_{-\infty}^{\infty} C(\tau) e^{-i\omega\tau} d\tau, \quad (A1)$$

where $C(\tau)$ is the velocity autocorrelation function

$$C(\tau) = \langle \mathbf{v}(0)\mathbf{v}(\tau) \rangle = \lim_{T \rightarrow \infty} \left[\frac{1}{T} \int_0^T \sum_{l=1}^N \mathbf{v}^l(t)\mathbf{v}^l(t+\tau) dt \right]. \quad (A2)$$

$\mathbf{v}^l(t)$ represents the velocity of atom l at time t for all N atoms of the system. As the calculation of the time averages $\langle \dots \rangle$ of Eq. (A2) is quite inefficient computationally, we use the Wiener-Khinchin theorem which guarantees that the power spectrum can also be calculated by individually Fourier transforming the velocities $\mathbf{v}^l(t)$ and summing the squares of the result:

$$I(\omega) = \frac{1}{N} \sum_{l=1}^N \left| \left[\frac{1}{2\pi} \int_{-\infty}^{\infty} \mathbf{v}^l(t) e^{-i\omega t} dt \right] \right|^2. \quad (A3)$$

Finite trajectories, calculated with a finite time step Δt , only yield estimates to the power spectrum. Instead of the Fourier integral in Eq. (A3), discrete Fourier sums have to be calculated according to

$$V_k^{l\mu} = \sum_{j=0}^{J-1} v_j^{l\mu} e^{\frac{2\pi i j k}{J}}, \quad (\text{A4})$$

where the $v_j^{l\mu}$ stand for the μ component ($\mu \in \{x, y, z\}$) of the velocity of atom l at time step j , and J is the number of time steps of the trajectory. The so-called periodogram estimate for the power spectrum is then defined for $J/2 + 1$ frequencies:⁷⁰

$$P^{l\mu}(0) = P^{l\mu}(f_0) = \frac{1}{J^2} |V_0^{l\mu}|^2,$$

$$P^{l\mu}(f_k) = \frac{1}{J^2} \left[|V_k^{l\mu}|^2 + |V_{J-k}^{l\mu}|^2 \right], \quad (\text{A5})$$

$$P^{l\mu}(f_c) = P^{l\mu}(f_{J/2}) = \frac{1}{J^2} |V_{J/2}^{l\mu}|^2.$$

The highest frequency $f_c = \frac{1}{2\Delta t}$ is called Nyquist frequency and is determined by the time step Δt of the MD calculation. Thus, the finite time estimate of the power spectrum can finally be written as

$$I^J(\omega) = \frac{1}{N} \sum_{l=1}^N \sum_{\mu=1}^3 P^{l\mu}(\omega). \quad (\text{A6})$$

The function $I^J(\omega)$ will approach the true power spectrum $I(\omega)$ of the system in the limit $J \rightarrow \infty$, *i.e.*, in the limit of infinitely long trajectories. The power spectrum estimates now provide us with information about the distribution of the vibrational energy of a molecule or a solid over the frequencies. Power spectra at different temperatures may be used to investigate the differences in the population of vibrational modes. The integral over the power spectrum corresponds to the kinetic energy of the system.

¹G. Joachim, J. K. Gimzewski, and A. Aviram, *Nature* **408**, 541 (2000).

²J. R. Heath, *Annu. Rev. Mater. Res.* **39**, 1 (2009).

³J. S. Miller and A. J. Epstein, *MRS Bull.* **25**, 21 (2000).

⁴F. Besenbacher, J. V. Lauritsen, and S. Wendt, *Nano Today* **2**, 30 (2007).

⁵S.-W. Hla and K.-H. Rieder, *Annu. Rev. Phys. Chem.* **54**, 307 (2003).

⁶R. Otero, F. Rosei, and F. Besenbacher, *Annu. Rev. Phys. Chem.* **57**, 497 (2006).

⁷A. Schwarz, D. Z. Gao, K. Lämmle, J. Grenz, M. B. Watkins, A. L. Shluger, and R. Wiesendanger, *J. Phys. Chem. C* **117**, 1105 (2013).

⁸S. Frabboni, G. C. Gazzadi, L. Felisari, and A. Spessot, *Appl. Phys. Lett.* **88**, 213116 (2006).

⁹S. Kim, D. Kulkarni, K. Rykaczewski, M. Henry, V. Tsukruk, and A. Fedorov, *IEEE Trans. Nanotechnol.* **11**, 1223 (2012).

¹⁰J. D. Wnuk, S. G. Rosenberg, J. M. Gorham, W. F. van Dorp, C. W. Hagen, and D. H. Fairbrother, *Surf. Sci.* **605**, 257 (2011).

¹¹S. J. Randolph, J. D. Fowlkes, and P. D. Rack, *Crit. Rev. Solid State Mater. Sci.* **31**, 55 (2006).

¹²N. Silvis-Cividjian, C. W. Hagen, and P. Kruij, *J. Appl. Phys.* **98**, 084905 (2005).

¹³F. Porrati, R. Sachser, and M. Huth, *Nanotechnology* **20**, 195301 (2009).

¹⁴I. Utke, P. Hoffmann, and J. Melngailis, *J. Vac. Sci. Technol. B* **26**, 1197 (2008).

¹⁵K. Muthukumar, R. Valentí, and H. O. Jeschke, *New J. Phys.* **14**, 113028 (2012).

¹⁶F. Salvat-Pujol, H. O. Jeschke, and R. Valentí, *Beilstein J. Nanotechnol.* **4**, 781 (2013).

¹⁷M. Huth, F. Porrati, C. Schwalb, M. Winhold, R. Sachser, M. Dukic, J. Adams, and G. Fantner, *Beilstein J. Nanotechnol.* **3**, 597 (2012).

¹⁸A. Botman, M. Hesselberth, and J. Mulders, *Microelectron. Eng.* **85**, 1139 (2008).

¹⁹J. Li, M. Toth, V. Tileli, K. A. Dunn, C. J. Lobo, and B. L. Thiel, *Appl. Phys. Lett.* **93**, 023130 (2008).

²⁰J. D. Barry, M. Ervin, J. Molstad, A. Wickenden, T. Brintlinger, P. Hoffmann, and J. Meingailis, *J. Vac. Sci. Technol. B* **24**, 3165 (2006).

²¹M. Huth, D. Klingenberg, C. Grimm, F. Porrati, and R. Sachser, *New J. Phys.* **11**, 033032 (2009).

²²Y. Widjaja and C. B. Musgrave, *Appl. Phys. Lett.* **80**, 3304 (2002).

²³S. M. George, *Chem. Rev.* **110**, 111 (2010).

²⁴L. Jeloica, A. Esteve, M. D. Rouhani, and D. Esteve, *Appl. Phys. Lett.* **83**, 542 (2003).

²⁵T. Aaltonen, A. Rahtu, M. Ritala, and M. Leskel, *Electrochem. Solid-State Lett.* **6**, C130 (2003).

²⁶Y. Xu and C. B. Musgrave, *Chem. Mater.* **16**, 646 (2004).

²⁷A. Y. Timoshkin, H. F. Bettinger, and H. F. Schaefer, *J. Phys. Chem. A* **105**, 3240 (2001).

²⁸A. Y. Timoshkin, H. F. Bettinger, and H. F. Schaefer, *J. Phys. Chem. A* **105**, 3249 (2001).

²⁹J. Shen, K. Muthukumar, H. O. Jeschke, and R. Valentí, *New J. Phys.* **14**, 073040 (2012).

³⁰K. Muthukumar, I. Ophale, J. Shen, H. O. Jeschke, and R. Valentí, *Phys. Rev. B* **84**, 205442 (2011).

³¹K. Muthukumar, H. O. Jeschke, R. Valentí, E. Begun, J. Schwenk, F. Porrati, and M. Huth, *Beilstein J. Nanotechnol.* **3**, 546 (2012).

³²P. Philippsen, E. Van Lenthe, J. Snijders, and E. Baerends, *Phys. Rev. B* **56**, 13556 (1997).

³³H. Steininger, S. Lehwald, and H. Ibach, *Surf. Sci.* **123**, 264 (1982).

³⁴S. Y. Chin, C. T. Williams, and M. D. Amiridis, *J. Phys. Chem. B* **110**, 871 (2006).

³⁵M. L. Smith, N. Kumar, and J. J. Spivey, *J. Phys. Chem. C* **116**, 7931 (2012).

³⁶P. E. Blöchl, *Phys. Rev. B* **50**, 17953 (1994).

³⁷G. Kresse and D. Joubert, *Phys. Rev. B* **59**, 1758 (1999).

³⁸G. Kresse and J. Hafner, *Phys. Rev. B* **47**, 558 (1993).

³⁹G. Kresse and J. Furthmüller, *Phys. Rev. B* **54**, 11169 (1996).

⁴⁰G. Kresse and J. Furthmüller, *Comput. Mater. Sci.* **6**, 15 (1996).

⁴¹J. Hafner, *J. Comput. Chem.* **29**, 2044 (2008).

⁴²Z.-Q. Liu, K. Mitsuishi, and K. Furuya, *Jpn. J. Appl. Phys.* **46**, 6254 (2007).

⁴³M. Weber, M. Rudolph, J. Kretz, and H. W. P. Koops, *J. Vac. Sci. Technol. B* **13**, 461 (1995).

⁴⁴O. Treutler and R. Ahlrichs, *J. Chem. Phys.* **102**, 346 (1995).

⁴⁵P. Deglmann, K. May, F. Furche, and R. Ahlrichs, *Chem. Phys. Lett.* **384**, 103 (2004).

⁴⁶K. Eichkorn, O. Treutler, H. Öhm, M. Häser, and R. Ahlrichs, *Chem. Phys. Lett.* **242**, 652 (1995).

⁴⁷K. Eichkorn, F. Weigend, O. Treutler, and R. Ahlrichs, *Theor. Chem. Acc.* **97**, 119 (1997).

⁴⁸Y.-I. Ishikawa, private communication (2012).

⁴⁹K. P. Reddy and T. L. Brown, *J. Am. Chem. Soc.* **117**, 2845 (1995).

⁵⁰Y.-I. Ishikawa and K. Kawakami, *J. Phys. Chem. A* **111**, 9940 (2007).

⁵¹*Photoprocesses in Transition Metal Complexes, Biosystems and other Molecules. Experiment and Theory*, NATO Science Series C, edited by E. Kochanski (Kluwer Academic Publishers, 1991).

⁵²K. M. Rao, G. Spoto, and A. Zecchina, *J. Catal.* **113**, 466 (1988).

⁵³K. Finnie, J. Thompson, and R. Withers, *J. Phys. Chem. Solids* **55**, 23 (1994).

⁵⁴J. B. Bates, *J. Chem. Phys.* **57**, 4042 (1972).

⁵⁵Y. Liang, C. R. Miranda, and S. Scandolo, *J. Chem. Phys.* **125**, 194524 (2006).

⁵⁶S. Coh and D. Vanderbilt, *Phys. Rev. B* **78**, 054117 (2008).

⁵⁷R. F. Howe, *Inorg. Chem.* **15**, 486 (1976).

⁵⁸A. Zecchina, E. Escalona Platero, and C. Otero Arean, *Inorg. Chem.* **27**, 102 (1988).

⁵⁹M. Suvanto and T. A. Pakkanen, *J. Mol. Catal. A: Chem.* **138**, 211 (1999).

⁶⁰K. M. Rao, G. Spoto, E. Guglielminotti, and A. Zecchina, *J. Chem. Soc. Faraday Trans.* **184**, 2195 (1988).

⁶¹R. L. Schneider, R. F. Howe, and K. L. Watters, *Inorg. Chem.* **23**, 4593 (1984).

- ⁶²S. Suvanto, T. A. Pakkanen, and L. Backman, *Appl. Catal. A: Gen.* **177**, 25 (1999).
- ⁶³P. J. Kenny, B. R. King, and H. F. Scheaefer, *Inorg. Chem.* **40**, 900 (2001).
- ⁶⁴B. Domenichini, J. Prunier, M. Petukov, Z. Li, P. J. Moller, and S. Bourgeois, *J. Electron Spectrosc. Relat. Phenom.* **163**, 19 (2008).
- ⁶⁵A. Zecchina and C. O. Aran, *Catal. Rev.* **35**, 261 (1993).
- ⁶⁶R. Cordoba, J. Sese, M. R. Ibarra, and J. M. De Teresa, *Appl. Surf. Sci.* **263**, 242 (2012).
- ⁶⁷H. O. Jeschke, "Theory for optically created nonequilibrium in covalent solids," Ph.D. thesis (Freie Universität Berlin, 2000).
- ⁶⁸X. Y. Chang, T. D. Sewell, L. M. Raff, and D. L. Thompson, *J. Chem. Phys.* **97**, 7354 (1992).
- ⁶⁹D. W. Noid, M. L. Koszykowski and R. A. Marcus, *J. Chem. Phys.* **67**, 404 (1977).
- ⁷⁰W. H. Press, S. A. Teukolsky, W. T. Vetterling, and B. Flanery, *Numerical Recipes: The Art of Scientific Computing*, 3rd ed. (Cambridge University Press, 2007).